Direct Observation of Nuclear Spin Diffusion in Real Space

Kai W. Eberhardt,[1] Schahrazede Mouaziz,[2] Giovanni Boero,[2] Jürgen Brugger,[2] and Beat H. Meier[1,*]

[1]*Physical Chemistry, ETH Zurich, CH-8093 Zurich, Switzerland*

[2]*Microsystems Laboratory, Ecole Polytechnique Fédérale de Lausanne (EPFL), Lausanne 1015, Switzerland*

(Received 8 August 2007; published 30 November 2007)

Images directly visualizing the spatial spin-diffusion process are reported. The measurements were performed using a magnetic resonance force microscope. The field gradient associated with the force-detection experiment is large enough to affect the spin dynamics and a modified kinetics of the spin-diffusion process is observed. The effects of the gradient were compensated for by a pulse scheme and a pure Zeeman diffusion rate constant of $D = (6.2 \pm 0.7) \times 10^{-12}$ cm^2/s in CaF_2 was observed.

DOI: 10.1103/PhysRevLett.99.227603 PACS numbers: 76.60.Pc, 68.37.Rt, 75.40.Gb

The concept of spin diffusion is of paramount significance in a variety of magnetic resonance experiments. It comprises the spatiotemporal transport of polarization in many-spin systems and was first introduced by Bloembergen in 1949 [1] to explain the unexpectedly fast spin-lattice relaxation in solids by diffusive transport of spin polarization to paramagnetic relaxation sinks. Spin diffusion is not only an interesting theoretical issue in many-body theory but is a key concept for many important applications, e.g., atomic-resolution structure determination of proteins [2], domain size determination in polymers and biopolymers [3,4], hyperpolarization of nuclei, e.g., in nanocrystals [5], to name a few.

Following the spin-diffusion (SD) process directly in space is a challenge because the rate constants are small and lead to transport over distances of the order of micrometers only, before the nuclear polarization has decayed due to spin-lattice (T_1) relaxation. For a long time, quantitative information about spin diffusion was only available through indirect measurements, e.g., of T_1 relaxation in diamagnetic systems doped by paramagnetic impurities [6]. Only recently, scattering experiments by Zhang and Cory [7] have provided a more direct experimental access to spin diffusion. Here we report the first direct observation of spin diffusion in real space by spatially and time-resolved magnetic resonance force microscopy (MRFM) [8].

The mechanism for spin diffusion is provided by mutual flip-flop processes of neighboring spins, induced by the magnetic dipole-dipole interaction. It is, even for many-spin systems, a coherent and deterministic process as demonstrated experimentally by time-reversal experiments [9]. Nevertheless, it is often adequate and useful to describe the SD process by an incoherent, diffusive mechanism. Theoretical studies which predict the SD rate constant from the crystal structure include the moment-method [10,11], perturbation approaches [12] and irreversible statistical mechanics [13]. Because the MRFM measurements take place in a strong field gradient, spin flip flops do not conserve the Zeeman energy even if they are, in the absence of the gradient, magnetically equivalent [14,15]. The attenuation of electron spin diffusion by stray field gradients, as reflected in modified T_1 relaxation times [16], was demonstrated by MRFM [17].

Our experiments were performed in a 6 T field at room temperature on ^{19}F spins in CaF_2. The rotating-frame Hamiltonian of the spin-system is dominated by the Zeeman and dipolar contributions, $\mathcal{H} = \mathcal{H}_Z + \mathcal{H}_d$, with

$$\mathcal{H}_Z(\mathbf{r}) = -\gamma \sum_j B(\mathbf{r}) I_{jz}, \tag{1}$$

$$\mathcal{H}_d = \frac{\mu_0 \gamma^2 \hbar}{4\pi} \sum_{kj,k<j} \frac{1 - 3\cos^2\theta_{kj}}{2r_{kj}^3} (3I_{kz}I_{jz} - \mathbf{I_k}\mathbf{I_j}), \tag{2}$$

where γ denotes the gyromagnetic ratio, r_{kj} the distance between nucleus k and j, and θ_{kj} the angle between the main field $\mathbf{B}(\mathbf{r})$ and the internuclear vector between spin k and j, $\mathbf{r}_{kj}$.

We consider the time evolution of a system described by an initial spin density operator of the form

$$\rho(\mathbf{r}) = e^{-\mathcal{H}(\mathbf{r})/kT}/Z \approx (1 - \beta_{Z,0}\mathcal{H}_Z - \beta_{d,0}\mathcal{H}_d)/Z, \tag{3}$$

where the $\approx$ sign stands for the high-temperature approximation. $Z = \mathrm{Tr}(e^{-\mathcal{H}(\mathbf{r})/kT})$ denotes the partition function and $\beta_Z = \frac{1}{k_b T_Z}$ and $\beta_d = \frac{1}{k_b T_d}$ the inverse spin temperatures of the Zeeman and dipolar bath, respectively [18]. The Zeeman and the dipolar baths will equilibrate with the lattice with the relaxation rate constants R_1 and R_{1d}, respectively.

In the absence of a field gradient β_Z and β_d are separate constants of the motion and Zeeman and dipolar polarization diffuse independently with diffusion rate constants D and D_d. In a field gradient, however, the mutual spin flip-flops are no longer energy conserving and the baths become coupled. For $|\nabla|\mathbf{B}||a \gg B_d$ the diffusion is quenched entirely, where a denotes the shortest internuclear distance, B is the static magnetic field and B_d is

the local field produced by the dipole interaction to all other spins in the sample. When $|\nabla|\mathbf{B}||a \ll B_d$, but the gradient $|\nabla|\mathbf{B}||$ is large enough to be noticeable in the diffusion path over the period of T_1, $|\nabla|\mathbf{B}||\sqrt{DT_1^2} \approx B_d$, the diffusion is merely reduced. This is the case we look at here.

Genack and Redfield derived the partial differential equations describing this process [14],

$$\frac{\partial}{\partial t}\beta_Z = D\nabla\left(\frac{\nabla(B\beta_Z)}{B} - \frac{D\nabla B}{B}\beta_d\right), \tag{4}$$

$$\frac{\partial}{\partial t}\beta_d = D_d\Delta\beta_d + \frac{D\nabla B}{B_d^2}(\nabla(B\beta_Z) - (\nabla B)\beta_d). \tag{5}$$

The magnetization associated with β_Z and β_d is $M_i = \beta_i CB$, the energy is $E_i = -\beta_i CB_i^2$, where $C = \frac{N_I}{3}I(I+1)\gamma_I^2\hbar$ is the Curie constant and N_I is the number of spins with spin quantum number I. Spin lattice relaxation can be incorporated into Eqs. (4) and (5) by adding the terms $-\frac{\beta_0-\beta_Z}{T_1}$ and $-\frac{\beta_0-\beta_d}{T_{1d}}$, respectively. For our experiments, Eqs. (4) and (5) can be simplified by replacing $\nabla(B\beta_Z)$ with $B\nabla\beta_Z$.

In the absence of a field gradient $\nabla B = 0$, the two Eqs. (4) and (5) are decoupled and Eq. (4) reduces to the well-known diffusion equation $\frac{\partial}{\partial t}\beta_Z = D\Delta\beta_Z$.

With the gradient, the time evolution of a magnetization profile starting with a step function at the origin ($\beta_Z(z) = \beta_0$ for $z \geq 0$ and $\beta_Z(z) = -\beta_0$ otherwise) can be divided into two time regimes. Initially the magnetization around $z = 0$ flows rapidly and tries to annihilate the step by equalizing the Zeeman spin temperatures. In a field gradient the energy mismatch for the flip-flop processes must be absorbed by the dipolar bath, which, due to its considerably smaller heat capacity, becomes polarized quickly and brings the diffusion process to a halt. At this point in time the diffusion has proceeded a distance such that the corresponding frequency shift is roughly equal to the dipolar coupling strength [$\frac{B_d}{|\nabla|\mathbf{B}||} \sim 30$ nm for $|\nabla|\mathbf{B}|| = 40\frac{\mathrm{G}}{\mu\mathrm{m}}$ and $B_d = 1.3$ G (vide infra)]. In the second time regime, further Zeeman spin diffusion becomes possible on a slower time scale thanks to spatial diffusion of the dipolar order. This process is described by the first term in Eq. (5) which changes the temperature of the dipolar bath and allows further Zeeman spin diffusion to take place. This slow process depends on the size of D_d, which is on the same order as D [11,19]. Only for $D_d \to \infty$ the Zeeman diffusion could proceed unhindered by the field gradient.

To measure the SD rate for Zeeman polarization in the presence of a field gradient, the bottleneck of the dipolar reservoir must be eliminated. This could be easily achieved by periodic inversions of the dipolar spin temperature. The dipolar energy, which tends to block the diffusion of the Zeeman magnetization before the inversion, will now drive the diffusion after the inversion [Eq. (4)]. If the inversions are applied faster than the buildup of dipolar energy the gradient will have no influence on the observed diffusion rate which is then identical to D. Experimentally, it is much simpler to realize periodic inversions of the Zeeman temperature while keeping the dipolar temperature constant. The influence on spin diffusion is the same. These inversions are simply achieved by adiabatic inversions of the ^{19}F spins corresponding to an inversion of β_Z.

The pulse sequence used for the measurements is shown in Fig. 1. A frequency-selective hyperbolic secant pulse [20] is used to generate a step function for the initial magnetization. This is followed by an evolution time with, optionally, a number of equally spaced inversion pulses. The short prepulse shown in the scheme does not influence the behavior of the spins. It only helps to reduce artifacts produced by the sudden heating of the cantilever caused by rf pulses. A Hadamard 16 scheme, described in detail elsewhere [21], is applied to improve the detection sensitivity. The signal is detected by adiabatic inversions from a triangular frequency modulated pulse, whose basic frequency matches the eigenfrequency of the cantilever. A more detailed description of our MRFM probe can be found in [22]. We use an iron cylinder as the gradient source (200 μm diameter, 10 mm length, $B_{\mathrm{sat}} = 1.75$ T). The single crystal CaF_2 sample was glued to the tip of a custom-made silicon cantilever [23] (500 nm thick, 350 μm long, 20 μm wide, $k = 2.4 \times 10^{-3}$ N/m, loaded

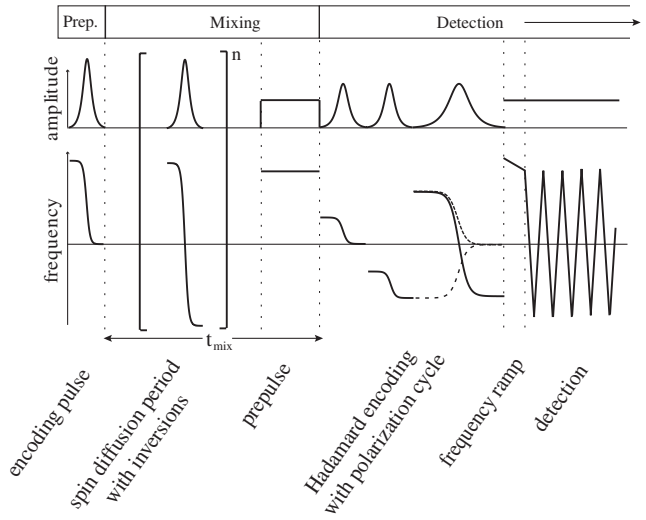

FIG. 1. Pulse sequence for spin-diffusion measurements. The first hyperbolic secant pulse inverts the magnetization over half of the field of view later acquired (step function). During the mixing time spin diffusion can proceed, optionally under the influence of n equally spaced refocusing pulses. The prepulse reduces artifacts from direct rf excitation of the cantilever. The mechanical detection is preceded by a Hadamard encoding step to increase the detection sensitivity [21] and finally obtained under triangular frequency sweeps with a period matched to the cantilever eigenfrequency for resonant excitation.

frequency $f_c = 832$ Hz and $Q \approx 30$ k). The crystal was ~ 25 μm in each dimension. Further details on the acquisiton parameters can be found in the supporting information [24]. The partial differential equations were numerically solved [25] with MATLAB (Mathworks, Inc.). The spatial derivatives of the magnetization at the end of the interval were set to zero to provide boundary conditions compatible with T_1 relaxation. The following parameters were used for all simulations: $B = 5.94$ T, $T_1 = 180$ s (120 s in the presence of refocusing pulses) and $|\nabla|\mathbf{B}||$ between 35 and 45 G/μm.

The diffusion of magnetization in the presence of the field gradient is shown in Fig. 2. The black data points in Figs. 2(a) and 2(b) are read out immediately after the inversion of half of the field of view. The initial condition (black circles) for the spin-diffusion process is a step function. Images of the magnetization, recorded 15.5 and 64.5 s after the inversion (in the absence of refocusing pulses), are given in Fig. 2(a). Spin diffusion tends to equilibrate the spin temperature and the step function broadens. The influence of T_1 relaxation manifests itself in the spectra by a reduction of the step size, also in the regions not influenced by diffusion.

The time evolution under inversion pulses is shown in Fig. 2(b). The experiments shown in the two figures use the same mixing times and clearly, spin diffusion proceeds significantly faster than in the experiment of Fig. 2(a). The inversion of the Zeeman spin temperature also leads to a different T_1 relaxation behavior, namely, a reduction in the step size. The center of the step function remains at zero magnetization.

In the absence of a field gradient, the time evolution of initial step function for the magnetization is given by the error function, which, including relaxation, is $M_z\{1 + e^{-(t_{\mathrm{mix}}/T_1)}[\mathrm{erf}(\frac{z}{\sqrt{4Dt_{\mathrm{mix}}}}) - 1]\}$. In the presence of the gradient, the situation becomes more complicated. As shown in the supporting information [24], the resulting profiles can still be well approximated with an error function, where the diffusion rate constant D is replaced by an effective diffusion constant D_{eff}. Because of the inversions the magnetization will decay to zero: $M_z e^{-(t_{\mathrm{mix}}/T_1)}\mathrm{erf}(\frac{z}{\sqrt{4Dt_{\mathrm{mix}}}})$.

In Fig. 2(c) the fitted D_{eff} for a spin-diffusion time of 15.5 s, is plotted as a function of the number of inversions. The experimental values given are statistical averages of the data from five positions in the crystal. The effective spin-diffusion rate approaches a value of $D_{\mathrm{eff}} = (6.2 \pm 0.7) \times 10^{-12}$ cm^2/s for a large number of inversion pulses. This value defines the Zeeman diffusion rate constant D. Using this value, all the experimental data of 2(a)–2(c) can be simultaneously fitted using the parameters $D_d = (11 \pm 11) \times 10^{-12}$ cm^2/s, $B_d = (1.3 \pm 0.3)$ G and $T_{1d} = (12 \pm 11)$ s. The simulations with these values are shown, as solid lines, in 2(a)–2(c). Clearly, all experimental data are in excellent agreement with the model. The experiment is, however, not very sensitive to parameters T_{1d} and D_d of the dipolar bath.

In Fig. 3 the time evolution of the dipolar spin temperature is simulated, using the same parameters as above. In Fig. 3(a) the rapid buildup of a sharp peak in the dipolar energy blocks the spin diffusion of the Zeeman polarization [see Eq. (4)], but when inversion pulses reverse the polarization gradient, the buildup is reversed as well, displayed in Fig. 3(b) and the coupling between dipolar and Zeeman bath averages out.

The data presented are the first direct observation, in real space, of nuclear spin diffusion in full spatiotemporal detail. The effect of the presence of a field gradient, where the Zeeman and dipolar diffusion become coupled and the dipolar bottleneck limits the diffusion rate, was directly observed. Periodic inversion of the Zeeman populations was demonstrated to remove this bottleneck and to allow

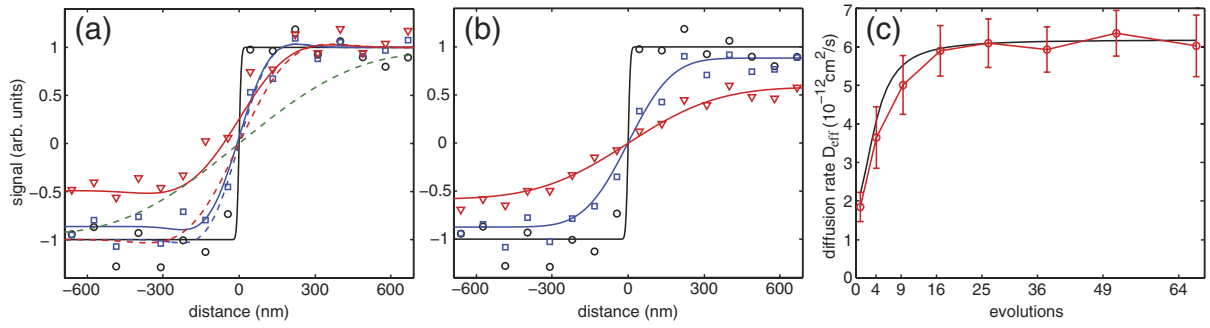

FIG. 2 (color online). (a) Spin diffusion in CaF_2 and (b) Inversion-driven spin diffusion for evolution times of 0, 15.5, and 64.5 s with 0, 15, and 63 inversions [black circles, blue (dark gray) boxes, and red (light gray) triangles, respectively]. The solid curves are simulations. Note that the overall amplitude of the experimental data was normalized to match the simulations, compensating for drift (largest scaling factor 1.4). The effects of spin diffusion are much stronger in (b) than in (a). The dashed lines in part (a) are simulations of the experiment without spin-lattice relaxation for 15.5, 64.5, and 600 s mixing time, respectively. (c) Dependence of the effective spin-diffusion rate D_{eff} on the number of inversion pulses during a constant mixing time of 15.5 s. The black curve is a simulation fitted to the experimental data [red (gray) circles]. With more pulses the spins diffusion is inhibited less by the gradient.

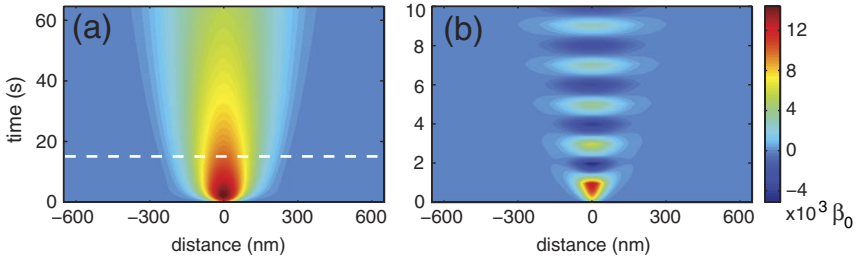

FIG. 3 (color online). Time evolution of the inverse dipolar spin temperature β_d during the experiment described in Fig. 2. Part (a) shows the evolution without inversions. The white line emphasizes the spatial scan at 15.5 s for which the Zeeman polarization is shown in Fig. 2(a). The step in the magnetization initially polarizes the dipolar reservoir. This blocks the diffusion of Zeeman polarization. Further time evolution is dictated by the diffusion of dipolar order. Part (b) shows the inverse dipolar spin temperature when the magnetization is inverted approximately every second (b). This inversion reverses the direction of the magnetization gradient and now the prior buildup of dipolar energy drives further Zeeman diffusion.

for spin diffusion independent of the field gradient. The rate constant obtained in these experiments ($D_{\text{eff}} = (6.2 \pm 0.7) \times 10^{-12}$ cm^2/s) matches the values (obtained without gradient) in the literature [7] with rate constants between 5.3 and 7.1 $\times 10^{-12}$ cm^2/s depending on the crystal orientation and theoretical values spanning 5.0 to 8.2 $\times 10^{-12}$ cm^2/s [11,13,26] very well.

We envision that similar measurements can be applied for the characterization of materials heterogeneous on the micrometer scale, e.g., polymers and biopolymers. The experiments should also be suited to follow other diffusion processes, e.g., proton diffusion in proton conductors or molecular diffusion, e.g., in water containing systems.

We thank the Schweizerischer Nationalfonds (SNF), the ETH Zurich, and the Kommission für Technologie und Innovation (KTI) for financial support. We thank Urban Meier and Andreas Hunkeler for their support with the setup and Christian Degen for fruitful discussions.

*beme@ethz.ch

[1] N. Bloembergen, Physica (Amsterdam) **15**, 386 (1949).
[2] F. Castellani, B. van Rossum, A. Diehl, M. Schubert, K. Rehbein, and H. Oschkinat, Nature (London) **420**, 98 (2002).
[3] T. T. P. Cheung, Phys. Rev. B **23**, 1404 (1981).
[4] J. Clauss, K. Schmidt-Rohr, and H. W. Spiess, Acta Polym. **44**, 1 (1993).
[5] P. vanderWel, K.-N. Hu, J. Lewandowski, and R. Griffin, J. Am. Chem. Soc. **128**, 10 840 (2006).
[6] G. W. Leppelmeier and J. Jeener, Phys. Rev. **175**, 498 (1968).
[7] W. R. Zhang and D. G. Cory, Phys. Rev. Lett. **80**, 1324 (1998).
[8] J. A. Sidles, Appl. Phys. Lett. **58**, 2854 (1991); J. A. Sidles, Phys. Rev. Lett. **68**, 1124 (1992).
[9] S. Zhang, B. H. Meier, and R. R. Ernst, Phys. Rev. Lett. **69**, 2149 (1992).
[10] A. G. Redfield, Phys. Rev. **116**, 315 (1959).
[11] A. G. Redfield and W. N. Yu, Phys. Rev. **169**, 443 (1968); A. G. Redfield and W. N. Yu, Phys. Rev. **177**, 1018 (1969).
[12] I. J. Lowe and S. Gade, Phys. Rev. **156**, 817 (1967); I. J. Lowe and S. Gade, Phys. Rev. **166**, 934 (1968); I. J. Lowe and S. Gade, Phys. Rev. B **5**, 3370 (1972).
[13] P. Borckmans and D. Walgraef, Phys. Rev. **167**, 282 (1968).
[14] A. Z. Genack and A. G. Redfield, Phys. Rev. B **12**, 78 (1975).
[15] G. B. Furman and S. D. Goren, Phys. Rev. B **68**, 064402 (2003).
[16] G. P. Berman, B. M. Chernobrod, V. N. Gorshkov, and V. I. Tsifrinovich, Phys. Rev. B **71**, 184409 (2005).
[17] R. Budakian, H. J. Mamin, and D. Rugar, Phys. Rev. Lett. **92**, 037205 (2004).
[18] A. G. Redfield, Phys. Rev. **98**, 1787 (1955); D. A. McArthur, E. L. Hahn, and R. E. Walstedt, Phys. Rev. **188**, 609 (1969); M. Goldman, *Spin Temperature and Nuclear Magnetic Resonance in Solids* (Clarendon, Oxford, 1970); C. P. Slichter, *Principles of Magnetic Resonance* (Springer-Verlag, Berlin, 1978).
[19] G. S. Boutis, D. Greenbaum, H. Cho, D. G. Cory, and C. Ramanathan, Phys. Rev. Lett. **92**, 137201 (2004).
[20] M. S. Silver, R. I. Joseph, C.-N. Chen, V. J. Sank, and D. I. Hoult, Nature (London) **310**, 681 (1984).
[21] K. W. Eberhardt, C. L. Degen, and B. H. Meier Phys. Rev. B **76**, 180405(R) (2007).
[22] C. L. Degen, Q. Lin, A. Hunkeler, U. Meier, M. Tomaselli, and B. H. Meier, Phys. Rev. Lett. **94**, 207601 (2005); C. L. Degen, U. Meier, Q. Lin, A. Hunkeler, and B. H. Meier, Rev. Sci. Instrum. **77**, 043707 (2006); D. Rugar, O. Zuger, S. Hoen, C. S. Yannoni, H. M. Vieth, and R. D. Kendrick, Science **264**, 1560 (1994).
[23] S. Mouaziz, G. Boero, G. Moresi, C. L. Degen, Q. Lin, B. H. Meier, and J. Brugger, Microelectron. Eng. **83**, 1306 (2006).
[24] See EPAPS Document No. E-PRLTAO-99-047747 for supplementary information. For more information on EPAPS, see http://www.aip.org/pubservs/epaps.html.
[25] R. D. Skeel and M. Berzins, SIAM J. Sci. Stat. Comput. **11**, 1 (1990).
[26] A. G. Redfield, Science **164**, 1015 (1969).